DELAYED DETACHED EDDY SIMULATION OF FLOW IN MACROSCALE AND MICROSCALE MULTI-INLET VORTEX REACTORS

Zhenping Liu

Department of Mechanical Engineering
Iowa State University
Ames, IA USA
payneliu@iastate.edu

Alberto Passalacqua

Department of Mechanical Engineering
Iowa State University
Ames, IA USA
albertop@iastate.edu

Michael G. Olsen

Department of Mechanical Engineering
Iowa State University
Ames, IA USA
mgolsen@iastate.edu

James C. Hill

Department of Chemical and Biological Engineering
Iowa State University
Ames, IA USA
jchill@iastate.edu

Rodney O. Fox

Department of Chemical and Biological Engineering
Iowa State University
Ames, IA USA
rofox@iastate.edu

ABSTRACT

The multi-inlet vortex reactor (MIVR) is used for flash nanoprecipitation to manufacture functional nanoparticles. A validated computational fluid dynamics model is needed for the design, scale-up, and optimization of the MIVR. Unfortunately, available Reynolds-averaged Navier-Stokes methods are unable to accurately model the highly swirling flow in the MIVR. Large-eddy simulations (LES) are also problematic, as excessively fine grids are required to accurately model this flow. These dilemmas led to the application of the dynamic delayed detached eddy simulation (DDES) method to the MIVR. In the dynamic DDES model, the eddy viscosity has a form similar to the Smagorinsky sub-grid viscosity in LES, which allows the implementation of a dynamic procedure to determine its model coefficient. Simulation results using the dynamic DDES model are found to match well with experimental data in terms of mean velocity and turbulence intensity, suggesting that the dynamic DDES model is a good option for modeling the turbulent swirling flow in the MIVR. By introducing a low Reynolds number turbulence model into the DDES formulation, it is possible to extend the applicability of the DDES model to transitional and weakly turbulent flow in a microscale MIVR.

INTRODUCTION

Chemical reactors for rapid mixing have been investigated intensively as they are required in certain precipitation reactions, including semi-batch stirred tank precipitators and impinging jet precipitators. The multi-inlet vortex reactor (MIVR) was originally designed as a microscale chemical reactor used to produce functional nanoparticles in the flash nanoprecipitation (FNP) technique where rapid mixing is required (Liu et al., 2008). The MIVR achieves fast mixing of streams from different inlets by inducing turbulent swirling flow into the reactor. The reactor consists of four inlets, one mixing chamber, and one outlet. Due to the arrangement of the inlets and the mixing chamber, the MIVR can provide good mixing at high Reynolds numbers and its mixing performance is insensitive to inlet flow rates of the individual streams. A natural question concerning the microscale MIVR is if it can be scaled up to larger dimensions without sacrificing its mixing performance (Marchisio et al, 2006). To answer this question, a scaled-up prototype of the MIVR has been built and investigated experimentally using stereoscopic particle image velocimetry (SPIV) (Liu et al., 2015). The experimental measurements reveal a number of interesting phenomena about the complex swirling flow in the MIVR. For example, a wandering motion of the vortex center was found to exist in the flow, and this wandering motion affects the measured turbulence kinetic energy and Reynolds stresses significantly. Despite the abundant information provided by the SPIV measurements, the understanding of the true three-dimensional structure of flow inside the reactor is still limited. Important parameters such as turbulent dissipation rate can only be obtained through approximations. A reliable numerical simulation of the scaled-up reactor is thus necessary to gain deeper understanding of the fundamental flow physics and to optimize the design and performance of the reactor.

The flow motion inside the MIVR is a turbulent swirling flow. The turbulence in such a swirling flow is difficult to model. These challenges are mainly caused by significant streamline curvature

existing in swirling flow. Streamline curvature affects turbulence structure by adding additional rate of strain into the flow, which in turn produces significant changes in turbulence kinetic energy production and distribution. These extra strain rates include lateral divergence, normal divergence, bulk compression, and rotation of whole flow system about the rotation (z) axis (Bradshaw, 1973). In the MIVR, flow undergoes helical motion towards the outlet. The sudden contracting geometry in the outlet of the MIVR also produces lateral and normal divergence. Thus all the additional strain rates except bulk compression will exist in the flow field of the MIVR, which makes successfully simulating the flow difficult.

The main problem with models using modified eddy viscosity is that they may only work for particular cases because these model coefficients are specifically tuned for a certain case. Hybrid RANS/LES is a promising method, which is able to improve the performance of RANS models while requiring less computational resources compared to LES (Gimbun et al., 2012). Detached eddy simulation (DES) falls into the category of hybrid RANS/LES methods. DES was originally developed to avoid the high grid requirement in LES by employing RANS in the near-wall region and an eddy-resolving simulation in regions away from the wall (Spalart et al, 1997). The original DES method could have artificial grid-induced separation when the eddy-simulation mode took place inside the boundary layer where the resolved Reynolds stresses have not replaced the modeled Reynolds stress (Menter and Kuntz, 1994). Delayed DES (DDES) was then proposed to solve this issue by using a shielding function to prevent the model from switching to eddy simulation near boundary layers (Spalart et al, 2006). Recently, Reddy et al. developed a new variant of the DDES model by clipping the length scale to the eddy viscosity in the $k-\omega$ model, making the eddy simulation more similar to LES (Reddy et al., 2014). Furthermore, Yin et al. implemented a dynamic procedure to compute the coefficient used in the eddy simulation, resulting in the dynamic DDES model. This dynamic DDES model adapts its coefficient according to how well turbulence is resolved, thus maximizing the resulting eddy-simulation region (Yin et al., 2015). Recent advances in the DDES model provide a powerful tool for simulating turbulent swirling flows, which can possess the accuracy of LES while having a computational cost closer to RANS.

In the current study, the dynamic DDES method is used to simulate flow inside the MIVR. A precursor simulation was first run to obtain the fully developed flow for the inlets of MIVR. Both steady and unsteady inlet conditions were tested for the simulation. The simulation results are validated by comparison with our SPIV measurements. The model is then extended to simulations for a microscale MIVR by introducing a low Reynolds number RANS formulation into the model. These results are compared to measurements from microPIV experiments.

MODELING APPROACH

The dimensionless filtered Navier-Stokes equations can be expressed as (repeated indices imply summation)

$$\frac{\partial \overline{u}_i}{\partial x_i} = 0 \qquad (1)$$

$$\frac{\partial \overline{u}_i}{\partial t} + \frac{\partial \overline{u}_i \overline{u}_j}{\partial x_j} = -\frac{\partial \overline{p}}{\partial x_i} + \frac{1}{\mathrm{Re}} \frac{\partial}{\partial x_j}\left(\frac{\partial \overline{u}_i}{\partial x_j}\right) - \frac{\partial \tau_{ij}}{\partial x_j} \qquad (2)$$

where τ_{ij} is the Reynolds-stress tensor in the RANS mode and turbulent sub-grid stress (SGS) tensor in the LES mode, and it is modeled as

$$\tau_{ij} = 2\nu_T S_{ij} - \frac{2}{3} k \delta_{ij} \qquad (3)$$

where S_{ij} is the mean strain-rate tensor. The dynamic DDES model (Yin et al., 2015) is based on clipping the production rate of the $k-\omega$ RANS model. In the DDES model, the turbulent eddy viscosity term in the $k-\omega$ model is replaced by the production of the square of the length scale and ω. When using the RANS length scale, the simulation runs in a RANS mode. However, if the length scale is the LES length scale, the simulation runs in an LES mode. Except for the wall area, the selection of the mode is determined by the magnitude of the RANS and LES length scales and, in principle, the smaller length scale is used. A shielding function is employed to ensure that the RANS mode will always be selected in the near-wall region. Here, the $k-\omega$ RANS model (Wilcox, 2006) given by

$$\frac{Dk}{Dt} = 2\nu_T |\boldsymbol{S}|^2 - C_\mu k\omega + \nabla \cdot \left[\left(\nu + \sigma_k (k/\omega)\right)\nabla k\right] \qquad (4)$$

$$\frac{D\omega}{Dt} = 2C_{\omega 1}|S|^2 - C_{\omega 2}\omega^2 + \nabla \cdot \left[\left(\nu + \sigma_\omega (k/\omega)\right)\nabla \omega\right] \qquad (5)$$

is used with the standard constants:

$$C_\mu = 0.09,\ \ \sigma_k = 0.5,\ \ \sigma_\omega = 0.5,\ \ C_{\omega 1} = 5/9,\ \ C_{\omega 2} = 3/40.$$

The only change in the current DDES model compared to the traditional $k-\omega$ RANS mode is the turbulent viscosity appearing in (4), which is defined by

$$\nu_T = l^2_{DDES}\omega,\ \ l_{DDES} = l_{RANS} - f_d \max(0, l_{RANS} - l_{LES}),\ \ l_{RANS} = \frac{\sqrt{k}}{\omega}, \qquad (6)$$

$$l_{LES} = C_{DES}\Delta,\ \ \Delta = f_d V^{1/3} + (1 - f_d) h_{\max}$$

where V is the cell volume, $h_{\max} = \max(dx, dy, dz)$ is the maximum cell spacing, and f_d is the DDES shielding function. It is worth mentioning that the equation for the grid size Δ helps alleviate the log layer mismatch problem. For this purpose, the shielding function is defined by

$$f_d = 1 - \tanh\left(\left[8 r_d\right]^3\right),\ \ r_d = \frac{k/\omega + \nu}{\kappa^2 d_w^2 \sqrt{U_{i,j}U_{i,j}}} \qquad (7)$$

where ν is the kinematic viscosity, κ the von Kármán constant, d_w the wall distance, and $U_{i,j}$ the velocity gradient tensor.

A dynamic procedure gives the empirical constant C_{DES} of the eddy simulation adaptively. This procedure also ensures that C_{DES} becomes a default number as the dynamic procedure is likely to fail on coarse meshes where the inertial range has not been resolved. Specifically, the dynamic procedure is defined as follows:

$$C_{DES} = \max(C_{lim},\ C_{dyn}),\ \ C^2_{dyn} = \max(0,\ 0.5\frac{L_{ij}M_{ij}}{M_{ij}M_{ij}}),$$

$$M_{ij} = \hat{\Delta}^2 \hat{\bar{\omega}} \hat{\bar{S}}_{ij} - \Delta^2 \widehat{\bar{\omega}\bar{S}_{ij}},\ \ L_{ij} = \hat{\bar{u}}_i \hat{\bar{u}}_j - \widehat{\overline{u_i u_j}} \qquad (8)$$

$$C_{lim}^2 = C_{DES}^0\left[1-\tanh\left(\alpha\exp\left(\frac{-\beta h_{\max}}{L_k}\right)\right)\right],\quad L_k=\left(\frac{\nu^3}{\varepsilon}\right)^{1/4}, \qquad (9)$$

$$\varepsilon = 2\left(C_{DES}^0 h_{\max}\right)^2\omega|S|^2 + C_\mu k\omega,\quad C_{DES}^0=0.12,\quad \alpha=25,\quad \beta=0.05$$

The dynamic DDES model was implemented into the open-source computational fluid dynamics (CFD) code OpenFOAM. A second-order, backward-difference method was used for time integration. Gradients were discretized with second-order accuracy, accounting for non-orthogonal corrections. The divergence scheme for k and ω is limited Linear, which is a central scheme with the Sweby limiter (Sweeby, 1984). The divergence terms for other variables are discretized using a second-order central scheme. The Laplacian scheme is second-order accurate. The generalized geometric-algebraic multi-grid (GAMG) solver is used as the linear system solver for the pressure equation and the Gauss-Seidel algorithm is used for other variables including velocity, k and ω. The solution for the system of partial conservation equations was obtained, at each time-step, by solving iteratively, to a specified tolerance of the residual norm.

The simulated geometry of the macroscale MIVR is shown in Fig. 1 (the simulation geometry for the microscale MIVR is identical, but is 1/16th this size). The outlet pipe has been made long enough to encompass any recirculation zones that may exist in the outlet. As the inlet channel in the experiment is about 870 mm long and is long enough for the inlet flow to fully develop, the inlet condition is modeled as fully developed for the reactor simulation. To obtain this developed inlet flow profile, a precursor simulation using a 160 mm long square duct was first conducted. The outflow is mapped back to the inlet so as to reach fully developed condition with relatively low computational cost. In each inlet, the bulk Reynolds number is 6580 and the dynamic DDES model is used as a turbulence model where grid resolution near the wall regions is fine enough so no wall functions must be used.

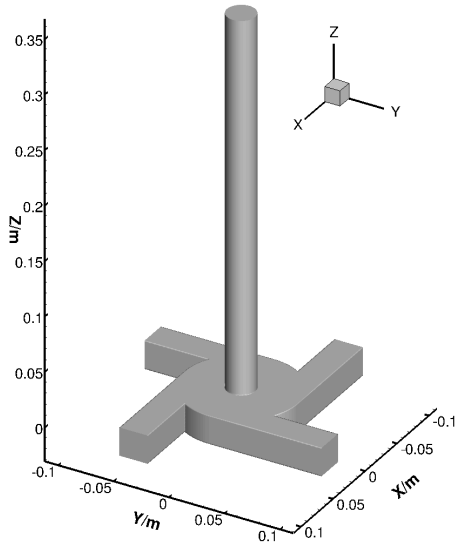

Figure 1. Simulation domain for the macroscale MIVR.

To simulate flow in the microscale MIVR, the dynamic DDES model was modified for use in transitional flow. This was done by first modifying the turbulent dissipation term in the standard k-ω model with a low Reynolds number correction. With this correction, the dynamic DDES model was found to handle flow at transitional Reynolds numbers very well.

RESULTS AND DISCUSSION

The streamlines of one typical instantaneous flow field in the macroscale MIVR from the simulation are presented in Fig. 2. The flow in the MIVR moves mainly in a helical motion. As can be seen in the streamlines at Z=0.06 m, this swirling motion is preserved quite well by the confined geometry and does not significantly dissipate as flow moves through the reactor. Vortex breakdown does not occur in the simulation domain. This phenomenon is different from the case where swirling flow enters a sudden expansion area. In a sudden expansion area, swirling motion decays much faster, and vortex breakdown is usually observed downstream of the expansion (Wang, 2004; Lu et al., 2005). The center of the swirling motion, i.e., the vortex center, also wanders around just as has been observed in other swirling flows (Ingvorsen et al., 2014). This wandering movement is found to be a small random motion rather than a preceding motion and no distinct frequency exists. In the streamlines at X=0 m, a low velocity area is observed near the center region where a recirculation appears. In other corner locations, small recirculation zones are also observed.

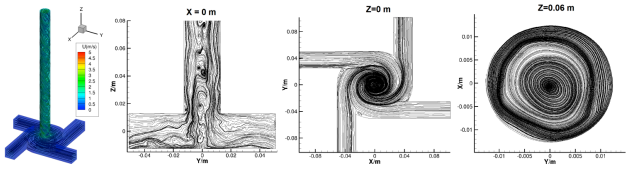

Figure 2. Instantaneous simulation velocity field in the MIVR (left: contour plot of velocity magnitude, middle left: vertical cross-section through center of outlet, middle right: horizontal cross-section through center of inlets, right: horizontal cross-section at outlet).

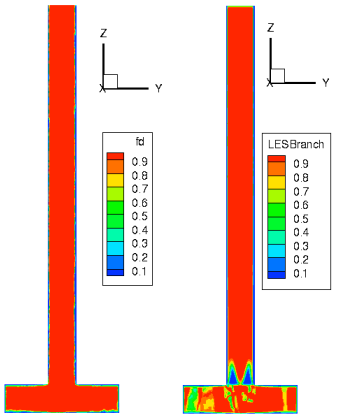

Figure 3. Dynamic DDES shielding function and eddy simulation branch on the center slice.

Figure 3 shows the contours of the shielding function, f_d, and the eddy-simulation region in the center slice of the simulation results. As is expected, the shielding function is close to zero near the wall and returns to one when it is away from the wall. This result guarantees the RANS mode will always be used near the wall. However, the selection of eddy-simulation mode away from

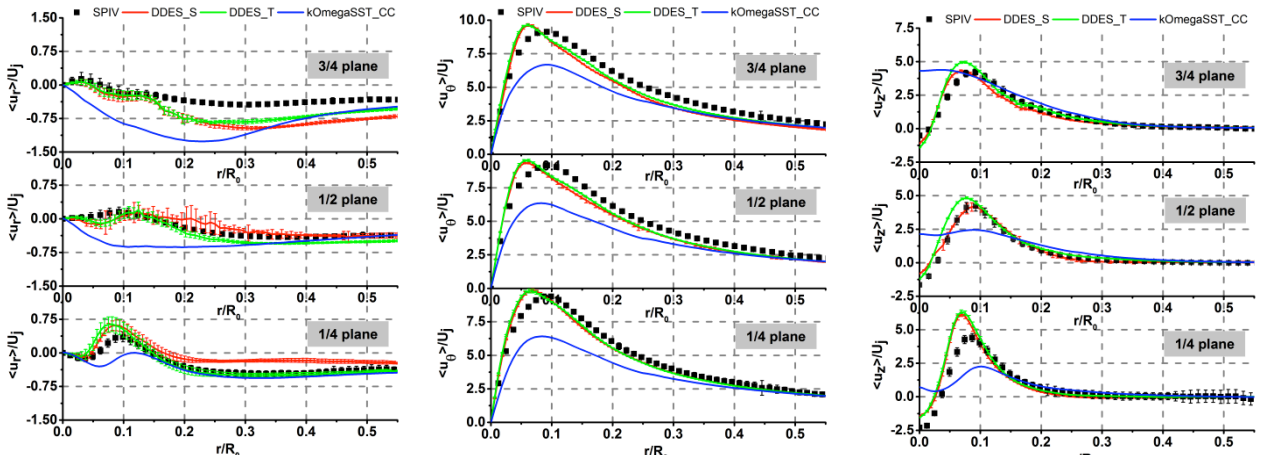

Figure 4. Mean radial, tangential and axial velocity-component profiles (left: $\overline{u}_r / U_j, \overline{u}_\theta / U_j, \overline{u}_z / U_j$) across reactor in three planes (top: ¾, middle: ½, bottom: ¼). Simulation results (lines: red – DDES_S, green – DDES_T, blue – k-omega) compared to SPIV data (symbols).

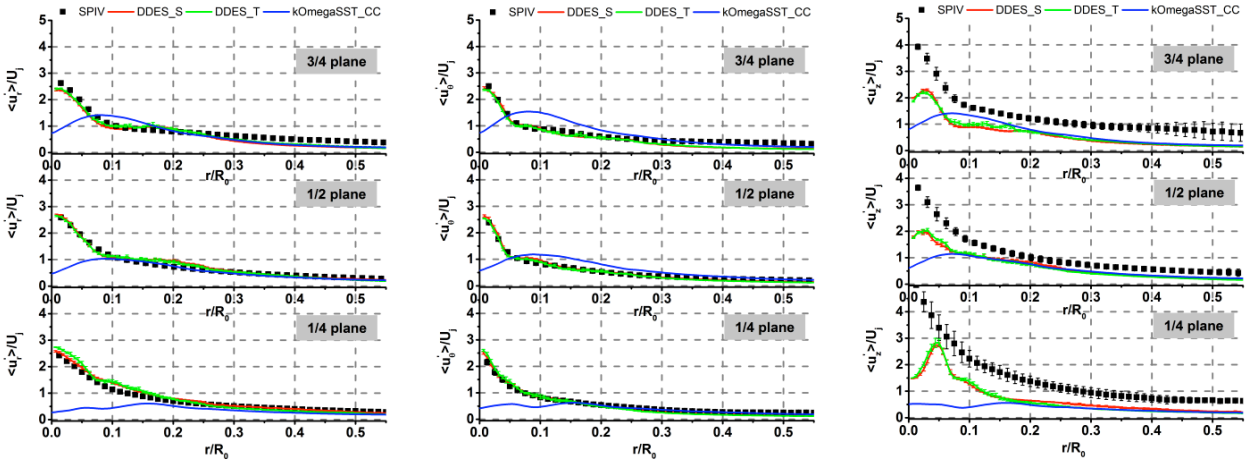

Figure 5. Normalized turbulence intensities (left: $< u_r' > /U_j, < u_\theta' > /U_j, < u_z' > /U_j$) across reactor in three planes (top: ¾, middle: ½, bottom: ¼). Simulation results (lines: red – DDES_S, green – DDES_T, blue – k-omega) compared to SPIV data (symbols).

the wall is determined by the ratio of the LES length scale, $C_{DES}\Delta$, over the RANS length scale, $\sqrt{k}/\omega$. For the current CFD work, not every location away from the wall has a grid fine enough to turn on the eddy-simulation mode, especially near the bottom of the outlet region. Although these RANS locations can be eliminated by further refining the mesh size, the main consideration here is to achieve accurate CFD predictions without consuming excessive computational resources, and thus such a grid refinement was not found to be necessary.

Figure 4 shows the radial distributions of the time-averaged radial, axial, and azimuthal velocity components at three measurement planes, z/H = 1/4, 1/2 and 3/4. The error bar at each point indicates the variance of the mean result that comes from performing this time average along different azimuthal angles. Simulation results using the dynamic DDES model with steady (DDES_S) and unsteady (DDES_T) inlets are compared with SPIV measurements. Overall, reasonable agreement is observed between simulations and experimental measurements. The dynamic DDES model with unsteady inlet conditions gives a better prediction for the mean velocity field, especially the radial velocity at the 1/4 plane. This is expected, as the unsteady inlet condition is closer to the physical situation and is thus usually recommended in an eddy simulation.

For comparison, simulations were also performed using the $k-\omega$ SST model with curvature correction, and this model did a fairly accurate job predicting the mean velocity in the region away from the center. However, near the reactor center, the azimuthal velocity is significantly underestimated and the declining trend of axial velocity cannot be captured. The RANS modeling tends to predict premature laminarization of the flow by adding excessive turbulent diffusion. The flow in the chamber is dominated by the azimuthal velocity, where peak radial velocity is much smaller than the other two components, and axial velocity is almost zero away from the center region ($r/R_0>0.3$). Based on the distribution of the azimuthal velocity, flow can be

divided into two main regions, a forced vortex region and a free vortex region. Near the reactor center, the azimuthal velocity corresponds to a forced vortex. Outside of the location of the peak azimuthal velocity, the azimuthal velocity resembles a free vortex.

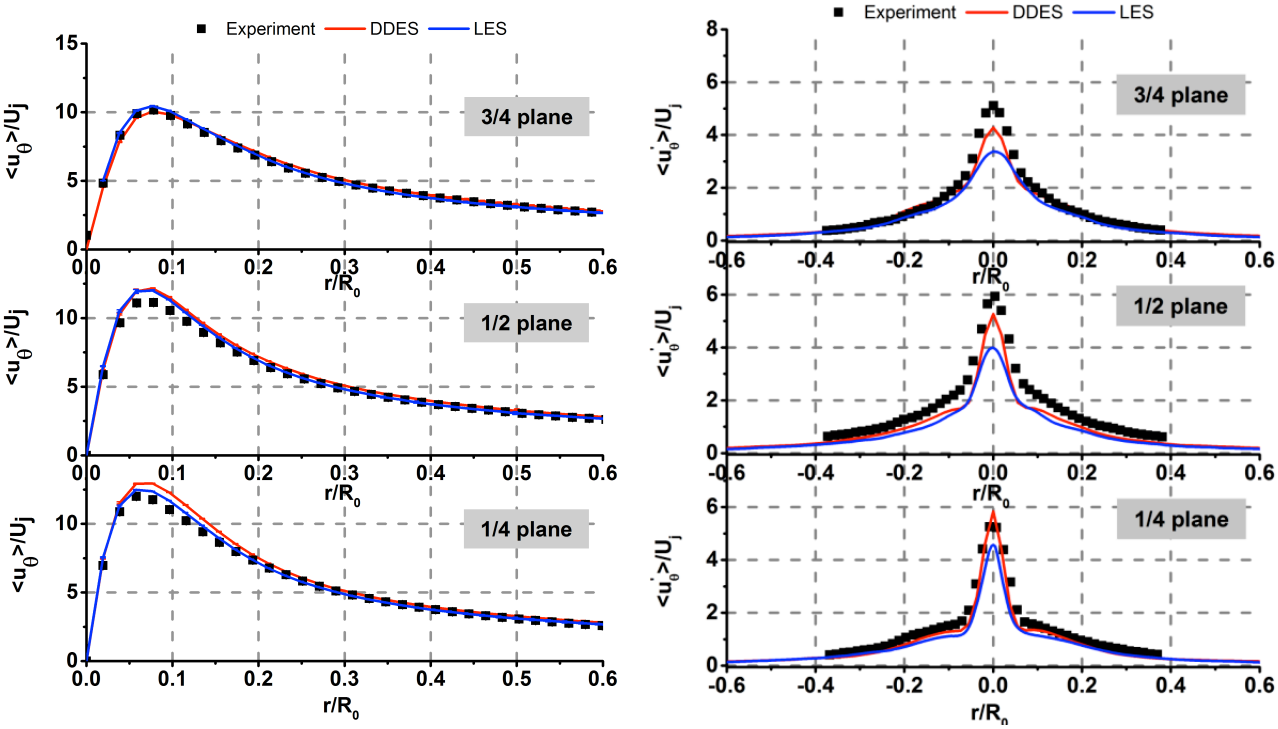

Figure 6. Comparison of mean velocity and turbulence intensity between the transitional DDES model, LES, and experimental data as measured by microPIV for the microscale MIVR.

It is observed that the mean axial velocity has similar profiles as the azimuthal velocity.

Figure 5 shows the radial distribution of normalized turbulence intensity components at three measurement planes, z/H = 1/4, 1/2 and 3/4. Again, the error bar at each point represents the variance of the mean result calculated along different azimuthal angles. The dynamic DDES model with steady (DDES_S) and unsteady (DDES_T) inlet conditions give almost the same predictions, indicating the fluctuation of inlet flow has little impact on the turbulence intensity of flow inside the chamber. Overall, reasonable agreement is observed between the simulation using dynamic DDES model and experimental results. The predicted radial and azimuthal turbulence intensities show good agreement with SPIV data. However, the axial turbulence intensity is underestimated in the simulations, especially near the reactor center. This discrepancy could be caused by the measurement noise in SPIV and the unsolved vortex core motion in simulation. Near the center of the reactor, the gradients of azimuthal and axial velocity become large, and in such high-gradient regions, the SPIV measurement could have high correlation noise (Doorne and Westerweel, 2006). This correlation noise could explain why high turbulence intensity is observed in the center area. When vortex core motion is not well captured, the predicted turbulent intensity will also deviate from experimental data. The $k-\omega$ SST model with curvature correction gives almost identical results as the dynamic DDES model in the region away from the center ($r/R_0>0.2$). However, it underestimates the turbulence intensities significantly near the center. The wandering motion of the vortex center and anisotropic features of turbulence seem to be the reasons causing the failure of the RANS simulation.

The measured turbulence intensity in the swirling flow within the macroscale MIVR can be attributed to both the pure turbulence phenomena and coherent structure bulk motion, i.e., precessing vortex core phenomenon or vortex wandering motion. The coherent structure motion tends to increase the measured turbulence intensity near the center of swirling flow. This contribution can be removed by freezing the vortex wandering motion during the calculation of turbulence intensity.[9] It is found that the vortex wandering motion mainly increases the radial and azimuthal turbulence intensities near the center. This finding suggests that the turbulence intensity near the vortex center should decrease if only the pure turbulence phenomenon is considered. This argument actually agrees with the streamline curvature effect on turbulence intensity. Turbulence will be stabilized in the forced vortex region by the mean velocity distribution while being destabilized in the free vortex region by the centrifugal force (Hreiz et al., 2011), just like the prediction by the $k-\omega$ SST model with curvature correction.

Figure 6 shows a comparison between the predictions of the transitional dynamic DDES model for the microscale MIVR with experimental results as measured by microPIV. The results of a large-eddy simulation are also presented for comparison. Excellent agreement is observed between the transitional DDES model. Indeed, the dynamic DDES model actually outperforms the LES model for this flow, especially in predicting turbulent velocity fluctuations while requiring only a fraction of the computational resources of LES.

CONCLUSIONS

Turbulent swirling flow in the macroscale MIVR is affected by both vortex wandering motion and streamline curvature, which makes a successful simulation difficult. In the current study, a dynamic DDES model was applied to model this flow. Both steady and unsteady inlet conditions are used and a small improvement of predicting the mean velocity is observed in the unsteady inlet case. Overall, the simulation results agree quite well with the experimental results in terms of the mean velocity and turbulence intensities. The recirculating backflow occurring at the center of MIVR is also captured by the dynamic DDES model. The existence of backflow is likely caused by the scale-up process and has not been reported previously in the microscale MIVR. The recirculation in the larger reactor could potentially cause a wider particle size distribution in the FNP technique and thus future work is needed to optimize the geometry of MIVR to eliminate the back mixing at the center. For comparison, a $k-\omega$ SST model with curvature correction has been used to simulate flow in the MIVR. Even with the curvature correction, the $k-\omega$ SST model is unable to accurately predict the flow field near the reactor center. As the vortex wandering and anisotropic turbulence features exist there, it is not surprising that the RANS model fails. The accuracy of the dynamic DDES model was shown to extend to the microscale MIVR when the dynamic DDES model is modified to be based a low Reynolds number RANS model. The superior performance of the dynamic DDES model confirms that it can reduce the drawbacks inherent to the RANS model and can be a good alternative for studying complex turbulent swirling flows.

REFERENCES

Bradshaw, P., 1973. Effects of streamline curvature on turbulent flow. *AGARD*. p. 131.

Doorne, C.W.H., Westerweel, J., 2006. Measurement of laminar, transitional and turbulent pipe flow using Stereoscopic-PIV. *Exp Fluids*., Vol. 42, pp. 259–279.

Gimbun, J., Rielly, C.D., Nagy, Z.K., Derksen, J.J., 2012. Detached eddy simulation on the turbulent flow in a stirred tank. *AIChE J*., Vol. 58, pp. 3224–3241.

Hreiz, R., Gentric, C., Midoux, N., 2011. Numerical investigation of swirling flow in cylindrical cyclones. *Chem Eng Res Des*., Vol. 89, pp. 2521–2539.

Ingvorsen, K.M., Meyer, K.E., Walther, J.H., Mayer, S., 2013. Turbulent swirling flow in a model of a uniflow-scavenged two-stroke engine. *Exp Fluids*., Vol. 54, pp.1494-1502.

Liu, Y., Cheng, C., Prud'homme, R.K., Fox, R.O. 2008. Mixing in a multi-inlet vortex mixer (MIVM) for flash nano precipitation. *Chem Eng Sci*., Vol. 63, pp. 2829–2842.

Liu, Z., Ramezani, M., Fox, R.O., Hill, J.C., Olsen, M.G., 2015. Flow characteristics in a scaled-up multi-inlet vortex nanoprecipitation reactor. *Ind Eng Chem Res*., Vol 54, pp. 4512–4525.

Lu, X., Wang, S., Sung, H.G., Hsieh, S.Y., Yang, V., 2005. Large-eddy simulations of turbulent swirling flows injected into a dump chamber., *J Fluid Mech*., Vol. 527, pp. 171–195.

Marchisio, D.L., Rivautella, L., Barresi, A.A., 2006. Design and scale-up of chemical reactors for nanoparticle precipitation. *AIChE J*., Vol. 52, pp. 1877–1887.

Menter, F.R., Kuntz, M., 1994. Adaptation of eddy-viscosity turbulence models to unsteady separated flow behind vehicles. *The Aerodynamics of Heavy Vehicles: Trucks, Buses, and Trains*, pp. 339–352.

Reddy, K.R., Ryon, J.A., Durbin, P.A., 2014. A DDES model with a Smagorinsky-type eddy viscosity formulation and log-layer mismatch correction. *Int J Heat Fluid Flow*., Vol. 50, pp.103–113.

Spalart, P.R., Jou, W.H., Strelets, M., Allmaras, S.R., 1997. Comments on the feasibility of LES for wings, and on a hybrid RANS/LES approach. *International Conference on DNS/LES*, pp. 137–147.

Spalart, P.R., Deck, S., Shur, M.L., Squires, K.D., Strelets, M.K., Travin, A., 2006. A new version of detached-eddy simulation, resistant to ambiguous grid densities. *Theor Comput Fluid Dyn*., Vol. 20, pp. 181–195.

Sweeby, P.K., 1984. High resolution schemes using flux limiters for hyperbolic conservation laws. *SIAM J Numer Anal*., Vol. 21, pp. 995–1011.

Yin, Z., Reddy, K.R., Durbin, P.A., 2015. On the dynamic computation of the model constant in delayed detached eddy simulation. *Phys Fluids*., Vol. 27, 025105.

Wang, P., Bai, X.S., Wessman, M., Klingmann, J., 2004. Large eddy simulation and experimental studies of a confined turbulent swirling flow. *Phys Fluids*., Vol. 16, pp. 3306–3324.

Wilcox, D.C., 2006. *Turbulence Modeling for CFD*. DCW Industries, Inc.